

Provided for non-commercial research and education use.
Not for reproduction, distribution or commercial use.



This article appeared in a journal published by Elsevier. The attached copy is furnished to the author for internal non-commercial research and education use, including for instruction at the authors institution and sharing with colleagues.

Other uses, including reproduction and distribution, or selling or licensing copies, or posting to personal, institutional or third party websites are prohibited.

In most cases authors are permitted to post their version of the article (e.g. in Word or Tex form) to their personal website or institutional repository. Authors requiring further information regarding Elsevier's archiving and manuscript policies are encouraged to visit:

<http://www.elsevier.com/copyright>



Nitrogen doping effects on the structure of graphene

Dongsheng Geng^a, Songlan Yang^{a,b}, Yong Zhang^a, Jinli Yang^a, Jian Liu^a, Ruying Li^a, Tsun-Kong Sham^b, Xueliang Sun^{a,*}, Siyu Ye^c, Shanna Knights^c

^a Department of Mechanical and Materials Engineering, University of Western Ontario, 1151 Richmond Street N., London, Ontario, Canada N6A 5B9

^b Department of Chemistry, University of Western Ontario, 1151 Richmond Street N., London, Ontario, Canada N6A 5B9

^c Ballard Power Systems Inc., 9000 Glenlyon Parkway, Burnaby, BC, Canada V5J 5J8

ARTICLE INFO

Article history:

Received 29 April 2011

Received in revised form 31 May 2011

Accepted 31 May 2011

Available online 7 June 2011

Keywords:

Graphene

Nitrogen doping

Defects

Structure

ABSTRACT

Graphene and nitrogen doped graphene have been prepared by modified Hummers' method and the following ammonia heat-treatment process, respectively. The effects of N-doping on the structure of graphene have been systematically investigated by various characterization techniques. SEM, TEM, BET, Raman and XRD analysis were used to distinguish the difference of the microstructures; and FT-IR, XPS, especially XANES were performed to elucidate the bonding information such as C–N. The effect of nitrogen doping on the structure of graphene has been obtained. More defects are present on nitrogen doped graphene as elucidated by BET, XRD, Raman, and XANES characterizations. XANES analysis also indicates that the N-doping decreases the surface oxygen-containing groups.

© 2011 Published by Elsevier B.V.

1. Introduction

Graphene, the two-dimensional (2D) monolayer of carbon atoms arranged in a honeycomb lattice, has recently attracted great interests for both fundamental and applied research since its discovery by Novoselov et al. [1] at the University of Manchester using the deceptively simple Scotch tape method. Graphene has unique physical and chemical properties, such as high surface area (theoretical value: $\sim 2630 \text{ m}^2 \text{ g}^{-1}$), high chemical stability, excellent conductivity (106 S cm^{-1} , higher than the conductivity of silver, the highest conductive substance known at room temperature), unique graphitic basal plane structure, and the easiness of functionalization and production. These unique physical and chemical properties lead graphene as an ideal base for applications in electric device [2], biosensors [3], field effect transistors [4], supercapacitors [5], lithium secondary batteries [6], and fuel cells [7–10]. Since material properties are always related to the structure of the material, many attempts have been made to modify the electrical properties of graphene by controlling its structure, which include preparing carbon sheets with different layers and graphene with and without defects by new synthesis methods [11,12], chemical functionalization of graphene [13–15], and chemical doping with foreign atoms

[16–18]. In general, chemical doping with N or B is considered an effective method to intrinsically modify the properties of carbon materials. Especially nitrogen doping plays a critical role in regulating the electronic and chemical properties of carbon materials due to its comparable atomic size and five valence electrons available to form strong valence bonds with carbon atoms. Theoretical study has shown that nitrogen doping results in the higher positive charge on a carbon atom adjacent to the nitrogen atoms [19], and a positive shift of Fermi energy at the apex of the Brillouin zone of graphene [20]. Some recent experimental results also proved that nitrogen doped graphene (N-graphene) has higher electrocatalytic activity for the reduction of hydrogen peroxide and oxygen than graphene [19,21]. Also, N-graphene has shown better performance in Li ion battery applications [22]. Furthermore, N-graphene as Pt support exhibited the higher electrocatalytic activity for methanol oxidation than graphene [23]. Therefore, it is of fundamental interest to investigate how nitrogen doping affects the structure of graphene and in turn the chemical properties can be adjusted accordingly. The question is then: what is the difference between the structure of graphene and N-graphene? Till date, however, only limited works have been done to investigate the structural difference between graphene and N-graphene [16,24,25]. Here, we report the results from a series of experiments designed and various advanced characterization techniques to address this question.

In this work, we prepared the N-graphene (2.8 at.% N content) by the heat-treatment of graphene under ammonia, and studied the effect of nitrogen doping on the structure of graphene systematically by various characterization techniques—BET (Brunauer,

* Corresponding author. Tel.: +1 519 6612111x87759; fax: +1 519 6613020.
E-mail address: xsun@eng.uwo.ca (X. Sun).

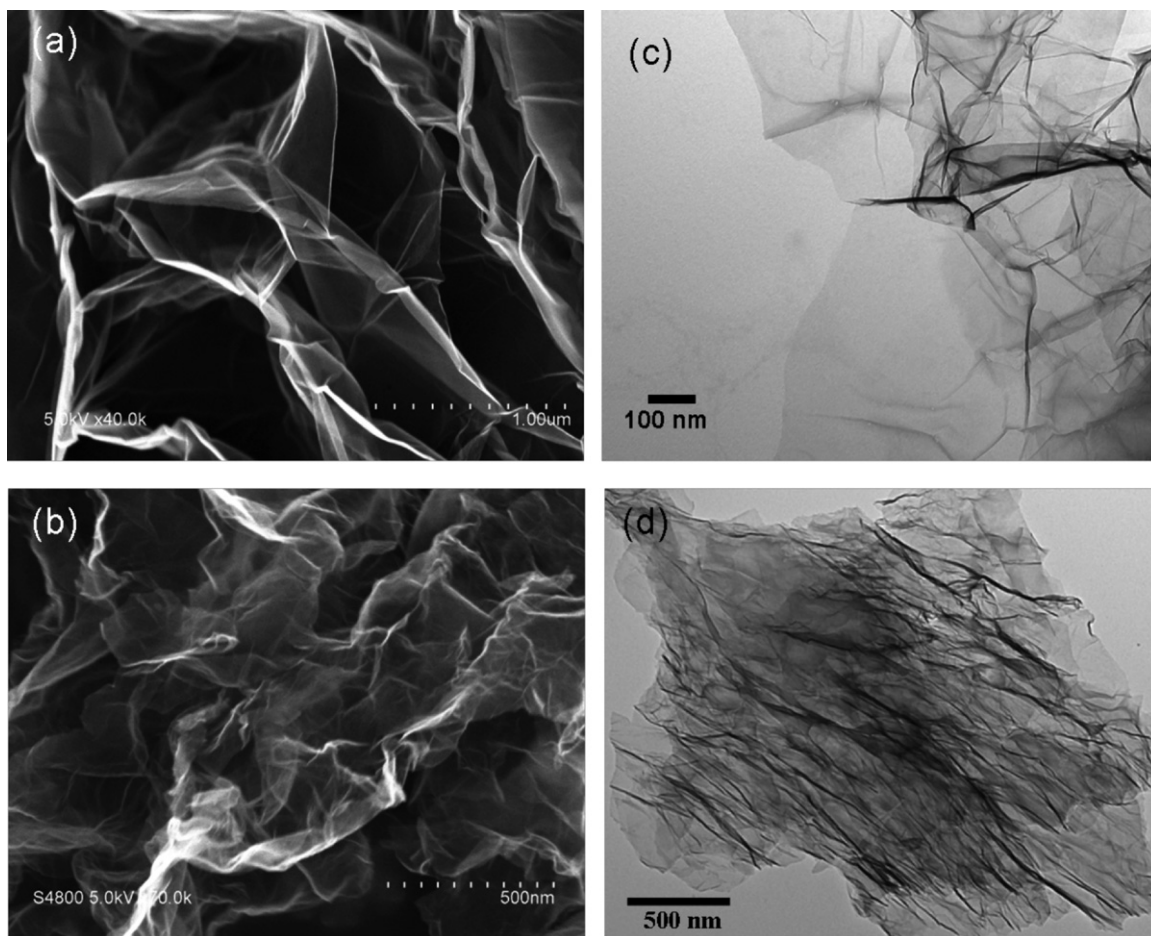


Fig. 1. SEM and TEM images of graphene (a and c) and N-graphene samples (b and d).

Emmett, and Teller) isotherm, scanning electron microscopy (SEM), transmission electron microscopy (TEM), X-ray diffraction (XRD), Raman spectra, FT-IR spectra, X-ray photoelectron spectroscopy (XPS), and X-ray absorption near-edge structure (XANES) spectroscopy.

2. Experimental

2.1. Preparation of graphene and N-graphene

Graphite powder was used as the starting material. Graphene was first prepared by the oxidation of graphite powder using the modified Hummers' method [26,27]. Typically, graphite powder (1 g) and sodium nitrate (0.75 g) were first stirred in concentrated sulphuric acid (37.5 mL) while being cooled in an ice water bath. Then potassium permanganate (4.5 g) was gradually added to form a new mixture. After 2 h in an ice water bath, the mixture was allowed to stand for five days at room temperature with gentle stirring. Thereafter, 100 mL of 5 wt% H₂SO₄ aqueous solution was added into the above mixture over 1 h with stirring. Then, 3 g of H₂O₂ (30 wt% aqueous solution) was also added to the above liquid and the mixture was stirred for 2 h. After that, the suspension was filtered and washed until the pH value of the filtrate was neutral. The as-received slurry is the so-called graphite oxide. Finally, the dried graphite oxide was heated at 1050 °C for 30 s under Ar to get graphene [28]. Nitrogen doped graphene was further obtained by heating the graphene under high purity ammonia mixed with Ar at 900 °C [29].

2.2. Physical characterizations

The morphologies of the samples were characterized by Hitachi S-4800 field-emission SEM operated at 5.0 kV, Philips CM10 TEM operated at 80 kV. BET is used to determine the specific surface area, pore size, and pore volume. Also the detailed structures have been characterized by XRD, Raman spectra, FT-IR spectra. The nitrogen contents for N-graphene was determined by Kratos Axis Ultra Al (alpha) XPS. The synchrotron-based XANES spectroscopy measurements were performed at the Canadian Light Source (CLS) on the High Resolution Spherical Grating Monochromator (SGM) beamline for the CK-, NK-, and OK-edge spectra. This beamline uses a 45 mm planar undulator and three gratings to cover a photon energy region from 250 to 2000 eV. It offers an energy resolution greater than 5000 $E/\Delta E$ at energy below 1500 eV [30]. The beamline is capable of providing 10¹² photons per second at 250 eV and exceeds 10¹¹ photons per second up to 1900 eV at 100 mA. Spectra were recorded in the fluorescence yield mode (FLY) using a microchannel-plate detector and the total electron yield (TEY) mode measuring the sample current. All spectra were normalized to the intensity of the incident beam (I_0), measured simultaneously as the current emitted from a gold mesh located after the last optical elements of the beamline.

3. Results and discussion

Fig. 1 shows the typical SEM and TEM images of graphene and N-graphene. It can be seen that the material is transparent with the

Table 1
Specific surface area of graphene and N-graphene determined by BET method.

Sample	Specific surface area ($\text{m}^2 \text{g}^{-1}$)	Pore volume ($\text{cm}^3 \text{g}^{-1}$)	Pore size (\AA)
Graphene	455.6	1.34	118.1
N-graphene	595.6	1.82	122.0

voile-like structure. These materials consist of randomly crumpled sheets closely associated with each other and forming a disordered solid. The graphene planar sheets are clearly observed in N-doped graphene, indicating that the features of high surface/volume ratio and the two-dimensional structure of graphene morphology are well maintained. However, it is hard to distinguish the difference between graphene and N-graphene from the general SEM and TEM observations.

Table 1 shows the detailed BET data for the two samples. It has been recently shown that graphene and N-graphene can be used as the catalysts or catalyst supports in fuel cells and batteries [10,23,31]. High specific surface area is thus usually required for the deposition of metals or metal oxides uniformly on these materials to enhance the (electro-) chemical activity. As one expects, the specific surface area increases from 455.6 to 595.6 $\text{m}^2 \text{g}^{-1}$ for graphene and N-graphene, respectively. The higher specific surface area is an indication of a higher degree of graphite exfoliation in the latter. However, it is still lower than the theoretical specific surface area for completely exfoliated and isolated graphene sheets, due to incomplete exfoliation and the agglomeration of graphene upon rapid heating. Also, one can notice that the pore volume and pore size increase slightly after nitrogen doping. During the preparation process of N-graphene, not only nitrogen atoms can substitute some carbon atoms that most likely located on the reactive edge [18], but ammonia also reacts with graphene to form hydrogen cyanide and hydrogen ($\text{C} + \text{NH}_3 = \text{HCN} + \text{H}_2$). This process consumed some carbon and may make the material more porous, which in turn resulted in the higher specific surface area, pore volume, and pore size.

In order to evaluate the degree of structural deformations of the graphene and N-graphene samples, Raman spectroscopy was carried out (Fig. 2). Two distinct peaks were observed. The D band, at approximately 1340 cm^{-1} for our samples, is disorder induced, attributable to structural defects and other disordered structures on the graphitic plane. The G band, at approximately 1570 cm^{-1} , is commonly observed for all graphitic structures and

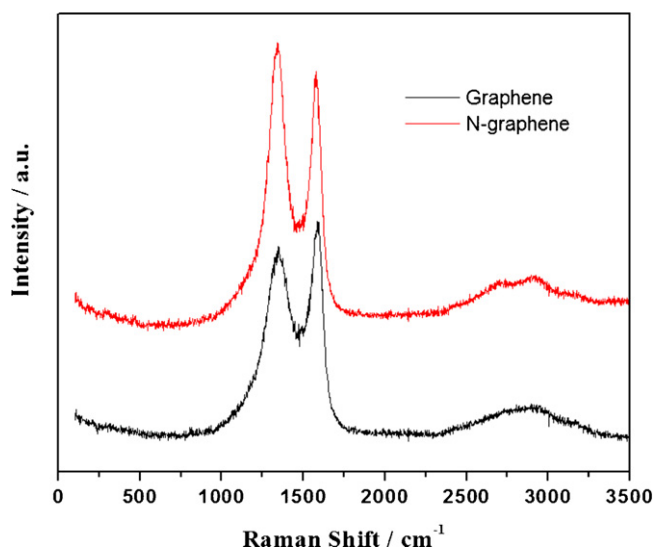


Fig. 2. Raman spectra of graphene and N-graphene samples.

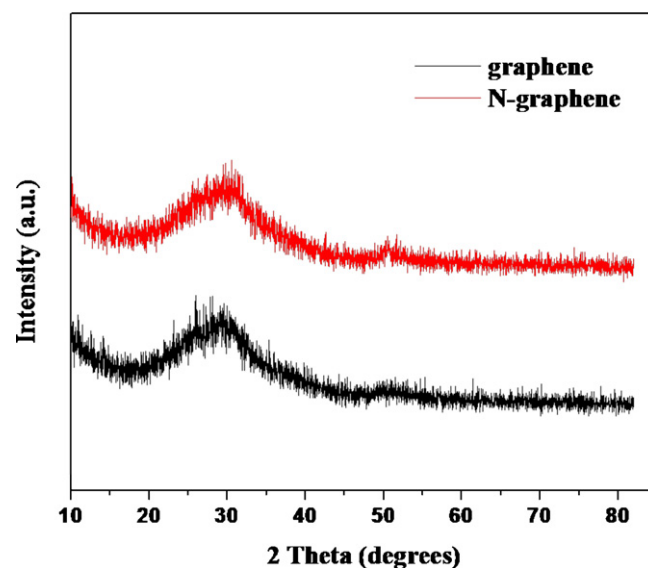


Fig. 3. XRD patterns of graphene and N-graphene samples.

can be attributed to the E_{2g} vibrational mode present in the sp^2 bonded graphitic carbons. The intensity ratio of D band to G band, namely the I_D/I_G ratio, provides the gauge for the amount of structural defects and a quantitative measure of edge plane exposure. N-graphene was found to have an I_D/I_G ratio of 1.12, obviously larger than 0.87 observed for graphene. The larger I_D/I_G ratio for N-graphene is a result of the structural defects and edge plane exposure caused by heterogeneous nitrogen atom incorporation into the graphene layers. The result is also consistent with our previous study about carbon nanotubes and N-doped carbon nanotubes [32].

Fig. 3 shows the XRD patterns for graphene and N-graphene. The pronounced (002) peaks at about 29.0° were seen for both samples, which are also assigned to the layer-to-layer distance (d -spacing: $d = \lambda/2 \sin \theta$). The average stacking number of a graphene layer was calculated [33] by using the d -spacing and size of the crystallite, which was evaluated from the width of the diffraction peak using the Scherrer equation ($\tau = K\lambda/\beta \cos \theta$, where K is the shape factor, λ is the X-ray wavelength, β is full width at half maximum intensity (FWHM) in radians, and θ is the Bragg angle; τ is the mean size of the crystalline domains). The detailed X-ray crystalline parameters are shown in Table 2. From these data, it can be seen that the interlayer spacing of graphene and N-graphene are larger than that of graphite (3.35 \AA); and the size of crystallite for N-graphene has slightly decreased compared with graphene, maybe due to ammonia corrosion and defects resulted from nitrogen doping. However, ammonia treatment process cannot affect the layers of graphene.

Furthermore, FT-IR spectra were used to investigate the bonding difference between graphene and N-graphene. From Fig. 4, it can be seen that although graphite oxide was reduced by rapid heating, the FT-IR spectrum of graphene still shows some characteristic bands of surface oxidized groups, at 3450 cm^{-1} (O–H stretching vibrations), at 1384 cm^{-1} (C–O–H stretching vibrations), and at 1100 cm^{-1} (C–O stretching vibrations) [34]. The peak located at 1635 cm^{-1} could be ascribed to the skeletal vibration of graphitic domains.

Table 2
X-ray structural parameters of graphene and N-graphene from plane (002).

Sample	θ , plane (002)	Value of d (\AA)	Value of τ (\AA)	No. of layers
Graphene	29.2	3.55	0.832	3.3
N-graphene	29.9	3.46	0.799	3.3

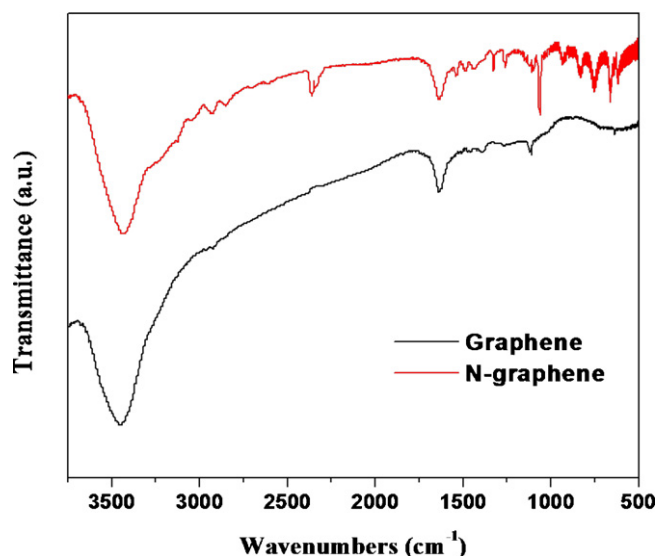


Fig. 4. Infrared spectra of graphene and N-graphene samples.

For N-graphene, in addition to the above-mentioned peaks, C–N stretching vibrations were observed at 1257 and 1326 cm^{-1} and N–H bend vibration at 1550 cm^{-1} was also obtained. Due to the overlap of peaks for C=C and C=N, and the relative low ratio of nitrogen to carbon atoms, it is difficult to prove the existence of C=N by FT-IR.

XPS, a powerful tool to identify the elements' states in bulk material, was thus used to prove the existence of C=N and other existing forms of nitrogen. XPS characterization (Fig. 5) indicated that about 2.8 at.% nitrogen was introduced to the graphene sheet by ammonia treatment under 900 °C. Based on the detailed analysis of N1s (insert, Fig. 5), the different proportion of pyridine-like N (398.1 eV), pyrrole-like N (399.9 eV), and quaternary N (401.3 eV) were observed. In addition, it was found that ammonia annealing temperature has the effect on N-doping content and the existence

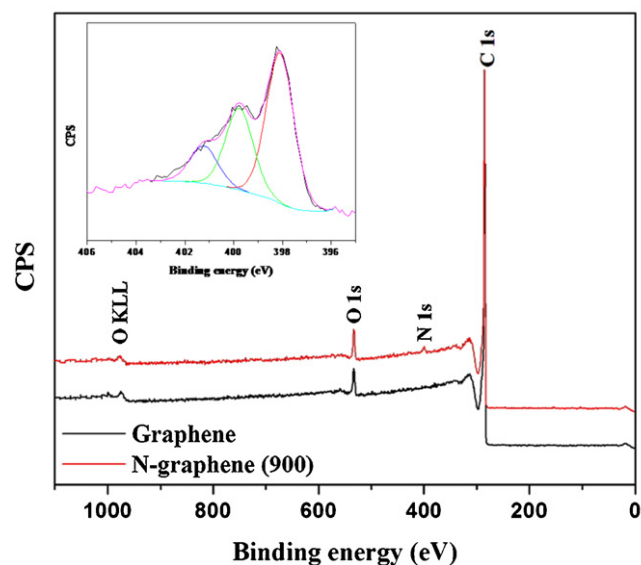


Fig. 5. XPS spectra of graphene and N-graphene samples. The inset: the high-resolution N1s spectra of N-graphene sample: the pink and black lines are the raw and fitted spectra. The red, green, and blue lines correspond to pyridine-like N (398.1 eV), pyrrole-like N (399.9 eV), and quaternary N (401.3 eV), respectively. (For interpretation of the references to color in this figure legend, the reader is referred to the web version of the article.)

forms of nitrogen. The N content is 2.8 and 2.0 at.% for N-graphene under 800 and 1000 °C annealing temperature, respectively. N-graphene under treatment temperature of 900 °C has the highest content of quaternary N, which is considered as the real doping [35]. Thus, it is clear that nitrogen was doped into the graphene structure.

XANES measurements were carried out to investigate the nitrogen doping effect in detail. CK-edge XANES spectra of graphene and N doped graphene are compared in Fig. 6(a). XANES spectroscopy is element specific and it concerns with the measurement and interpretation of the absorption coefficient above an absorption edge of an element in a chemical environment. At the C and NK-edge, the area under the resonance in the vicinity of the threshold in XANES (also called white line) is proportional to the unoccupied density of state (DOS) when tuneable X-rays are used to excite the 1s electron into previously unoccupied electronic states of p character (dipole selection rules). In graphite, the CK-edge will clearly exhibit a π^* (~ 285 eV) and a σ^* (~ 291 eV) resonance [36]. In high purity graphene, similar resonance patterns have been observed together with a well-defined peak at ~ 283.6 eV [37]. The region between the π^* and σ^* resonance is usually flat or monotonic if the samples are without impurity. For surface functionalized graphite, graphene, carbon nanotubes, resonance structures characteristic of oxygen or nitrogen functionalized surface groups will appear. For better comparison, the CK-edge spectra of graphene and N-graphene are normalized to the edge jump (where the absorption coefficient reaches at a flat region above the edge) of unity. At a first glance of Fig. 6(a), both spectra show two main features, the π^* transition at around 285.5 eV and the σ^* transition at around 291.7 eV, which is the signature of the graphitic structure. It should be noted that the relative intensity of the π^* vs. σ^* transition depends on the relative orientation of the graphitic plane with respect to the polarization of the incident photon, which is linearly polarized in the plane of the electron orbit of the synchrotron. At normal incidence, the σ^* dominates and at grazing incidence, the π^* dominates. In the present case, the angle of incidence was at 45°, and the sample is not perfectly flat, both resonances are noticeable. In between these two main features, a weak peak at 288.3 eV can also be detected in the undoped graphene, the intensity of which decreased obviously after N-doping. This feature has been previously characterized as the resonance from the π^* of the C=O bond of the carboxylic COOH group [38]. It is worth reiterating that no spectral feature in the region between the π^* and σ^* can be observed for high purity graphite, carbon nanotube and graphene with little defects. Another pre-edge feature centered at around 283.6 eV can also be detected in both cases. This feature is due to the surface defects, for example, dangling bonds [39] and amorphous carbon. The intensity for this pre-edge feature increased with N-doping. Therefore, with N-doping, more defect sites have been created in the graphene. Even though, those features from N related functional groups in between 287 and 288 eV cannot be easily discerned, the intensity for both π^* transition and σ^* transition increased a little after N-doping. This is a powerful evidence that after the N-doping the unoccupied DOS increased by the charge transfer from carbon to the more electronegative nitrogen, which is beneficial for the electric conductivity of the material.

The existence of N in the N-graphene can be confirmed by the corresponding TEY of the NK-edge XANES spectra as shown in Fig. 6(b). Three main peaks can be detected as centered at 397.9 eV, 400.7 eV and 406.3 eV. The first two features arise from transitions from the K shell (N1s) to unoccupied π^* orbital containing N character and the last is due to the transition into σ^* orbital [40]. They are undoubtedly a direct support of successful doping into the graphene matrix, forming unsaturated C–N bonds. The π^* resonance at 397.9 eV is attributed to the pyridine-like bonding in nitrogenated carbon materials, and the other broad peak from 399.3

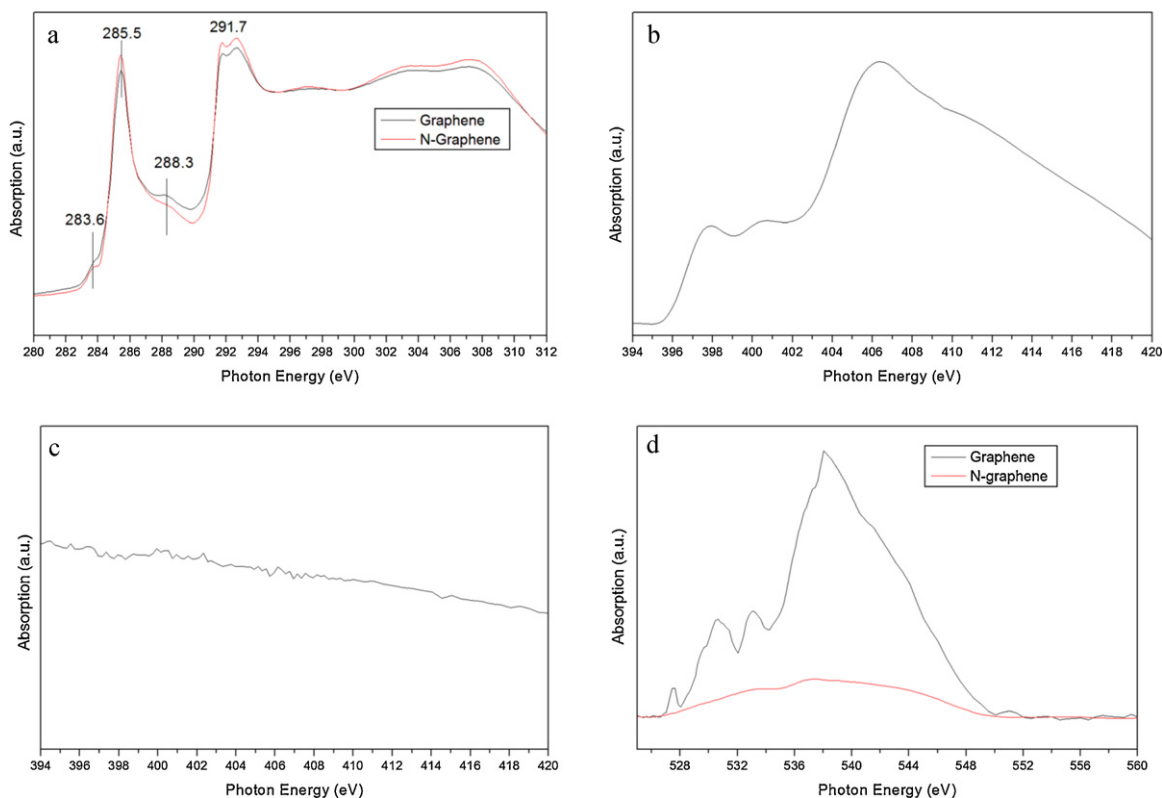


Fig. 6. (a and b) TEY of the CK-edge and NK-edge XANES spectra of graphene and N-doped graphene, (c) FLY of the XANES spectra of the N-doped graphene, and (d) TEY of the OK-edge XANES spectra of graphene and N-doped graphene.

to 401.7 eV may come from pyrrole- and graphite-like bonding. No signal from the NK-edge can be found through the bulk sensitive FLY, as shown in Fig. 6(c), therefore, the doping predominately occurred in the surface of graphene specimen under investigation.

The effect of N-doping on the content of oxygen-containing groups in graphene can be confirmed by the comparison of OK-edge as shown in Fig. 6(d). Several features corresponding to different oxygen-containing groups are visible from the graphene (the black line). The peak at 530.6 eV is from the π^* state of C=O, the one at 533.3 eV is related from to the π^* state of C(sp²)-O, and that at 536.3 eV belongs to the σ^* state of the C-O [41]. After N-doping, the peak intensity diminishes and the presence of those oxygen-containing groups once existed on the surface of undoped graphene is no longer evident.

4. Conclusions

Nitrogen doped graphene has been prepared by the heat-treatment of graphene using ammonia. XPS results indicated that about 2.8 at.% nitrogen was introduced into the graphene layer. The effects of N-doping on graphene have been systematically investigated by a number of techniques for microstructure and bonding studies. The results show that after nitrogen doping, the graphene basically maintains the initial morphology based on the SEM and TEM images. Most importantly, XANES confirms the incorporation of N into the graphene lattice. Several observations must be noted. First, these results show that there are several nitrogen species such as pyridine-like, pyrrole-like, pyridine-like, and quaternary N contents on the N-graphene. Second, after the N-doping, XANES results reveal that the unoccupied DOS increases, suggesting charge transfer from carbon to the more electronegative nitrogen, which is beneficial for the electric conductivity of the material. Finally, the N-doping decreases the surface oxygen-containing groups, which

may provide a new way to control the surface oxygen contents, and improve the corrosion resistance of graphene. In addition, BET analysis reveals that N-graphene has the increased specific surface area compared with graphene, indicating that more defects exist on the surface, which is supported by the observation of decreased size and higher I_D/I_G ratio after doping from XRD and Raman results, respectively. The resulting surface defects due to nitrogen doping is expected to enhance Li⁺ storage for Li ion battery applications and the anchoring of Pt nanoparticles on N-graphene for fuel cell electrocatalyst applications.

Acknowledgments

This research was supported by Natural Sciences and Engineering Research Council of Canada (NSERC), Ballard Power Systems Inc., Canada Research Chair (CRC) Program, Canada Foundation for Innovation (CFI), Ontario Research Fund (ORF), Ontario Early Researcher Award (ERA) and the University of Western Ontario. CLS is supported by CFI, NRC, NSERC, CIHR and the University of Saskatchewan.

References

- [1] K.S. Novoselov, A.K. Geim, S.V. Morozov, D. Jiang, Y. Zhang, S.V. Dubonos, I.V. Grigorieva, A.A. Firsov, *Science* 306 (2004) 666–669.
- [2] N. Levy, S.A. Burke, K.L. Meaker, M. Panlasigui, A. Zettl, F. Guinea, A.H. Castro Neto, M.F. Crommie, *Science* 329 (2010) 544–547.
- [3] Y. Shao, J. Wang, H. Wu, J. Liu, Aksay I.A., Y. Lin, *Electroanalysis* 22 (2010) 1027–1036.
- [4] F. Xia, D.B. Farmer, Y.-M. Lin, P. Avouris, *Nano Lett.* 10 (2010) 715–718.
- [5] L.L. Zhang, R. Zhou, X.S. Zhao, *J. Mater. Chem.* 20 (2010) 5983–5992.
- [6] E.J. Yoo, J. Kim, E. Hosono, H.-S. Zhou, T. Kudo, I. Honma, *Nano Lett.* 8 (2008) 2277–2282.
- [7] D.R. Kauffman, A. Star, *Analyst* 135 (2010) 2790–2797.
- [8] B. Seger, P.V. Kamat, *J. Phys. Chem. C* 113 (2009) 7990–7995.
- [9] L. Qu, Y. Liu, J.-B. Baek, L. Dai, *ACS Nano* 4 (2010) 1321–1326.

- [10] Y. Shao, S. Zhang, C. Wang, Z. Nie, J. Liu, Y. Wang, Y. Lin, J. Power Sources 195 (2010) 4600–4605.
- [11] A. Gupta, G. Chen, P. Joshi, S. Tadigadapa, P.C. Eklund, Nano Lett. 6 (2006) 2667–2673.
- [12] O.C. Compton, S.T. Nguyen, Small 6 (2010) 711–713.
- [13] K.P. Loh, Q. Bao, P.K. Ang, J. Yang, J. Mater. Chem. 20 (2010) 2277–2289.
- [14] D.W. Boukhvalov, M.I. Katsnelson, Nano Lett. 8 (2008) 4373–4379.
- [15] Y. Zhu, A.L. Higginbotham, J.M. Tour, Chem. Mater. 21 (2009) 5284–5291.
- [16] L.S. Panchakala, K.S. Subrahmanyam, S.K. Saha, A. Govindaraj, H.R. Krishnamurthy, U.V. Waghmare, C.N.R. Rao, Adv. Mater. 21 (2009) 1–5.
- [17] J.C. Meyer, S. Kurasch, H.-J. Park, V. Skakalova, D. Künzel, A. Groß, A. Chuvilin, S. Roth, U. Kaiser, Microsc. Microanal. 16 (Suppl. 2) (2010) 542–543.
- [18] X. Wang, X. Li, L. Zhang, Y. Yoon, P.K. Weber, H. Wang, J. Guo, H. Dai, Science 324 (2009) 768–771.
- [19] K. Gong, F. Du, Z. Xia, M. Duratock, L. Dai, Science 323 (2009) 760–764.
- [20] S.U. Lee, R.V. Belosludov, H. Mizuseki, Y. Kawazoe, Small 5 (2009) 1769–1775.
- [21] Y. Wang, Y. Shao, D.W. Matson, J. Li, Y. Lin, ACS Nano 4 (2010) 1790–1798.
- [22] A.L.M. Reddy, A. Srivastava, S.R. Gowda, H. Gullapalli, M. Dubey, P.M. Ajayan, ACS Nano 4 (2010) 6337–6342.
- [23] L.-S. Zhang, X.-Q. Liang, W.-G. Song, Z.-Y. Wu, Phys. Chem. Chem. Phys. 12 (2010) 12055–12059.
- [24] S.-F. Huang, K. Terakura, T. Ozaki, T. Ikeda, M. Boero, M. Oshima, J.-i. Ozaki, S. Miyata, Phys. Rev. B 80 (2009) 235410.
- [25] B. Guo, Q. Liu, E. Chen, H. Zhu, L. Fang, J.R. Gong, Nano Lett. 10 (2010) 4975–4980.
- [26] W.S. Hummers, R.E. Offeman, J. Am. Chem. Soc. 80 (1958) 1339.
- [27] M. Hirata, T. Gotou, S. Horiuchi, M. Fujiwara, M. Ohba, Carbon 42 (2004) 2929–2937.
- [28] H.C. Schniepp, J.-L. Li, M.J. McAllister, H. Sai, M. Herrera-Alonso, D.H. Adamson, R.K. Prud'homme, R. Car, D.A. Saville, I.A. Aksay, J. Phy. Chem. B 110 (2006) 8535–8539.
- [29] X. Li, H. Wang, J.T. Robinson, H. Sanchez, G. Diankov, H. Dai, J. Am. Chem. Soc. 131 (2009) 15939–15944.
- [30] <http://exshare.lightsource.ca/sgm/Pages/Beamline.aspx>.
- [31] S.-M. Paek, E.J. Yoo, I. Honma, Nano Lett. 9 (2009) 72–75.
- [32] H. Liu, Y. Zhang, R. Li, X. Sun, S. Désilets, H. Abou-Rachid, M. Jaidann, L.-S. Lussier, Carbon 48 (2010) 1498–1507.
- [33] B.K. Saikia, R.K. Boruah, P.K. Gogoi, J. Chem. Sci. 121 (2009) 103–106.
- [34] S. Stankovich, R.D. Piner, S.T. Nguyen, R.S. Ruoff, Carbon 44 (2006) 3342–3347.
- [35] D. Geng, Y. Chen, Y. Chen, Y. Li, R. Li, X. Sun, S. Ye, S. Knights, Energy Environ. Sci. 4 (2011) 760–764.
- [36] T.K. Sham, Int. J. Nanotechnol. 5 (2008) 1194–1246.
- [37] D. Pacilé, M. Papagno, A.F. Rodríguez, M. Grioni, L. Papagno, C.Ö. Girit, J.C. Meyer, G.E. Begtrup, A. Zettl, Phys. Rev. Lett. 101 (2008) 066806.
- [38] A. Kuznetsova, I. Poppva, J.T. Yates Jr., M.J. Bronikowski, C.B. Huffman, J. Liu, R.E. Smalley, H.H. Hwu, J.G. Chen, J. Am. Chem. Soc. 123 (2001) 10699–10704.
- [39] R. Gago, M. Vinnichenko, H.U. Jäger, A. Yu. Belov, I. Jiménez, N. Huang, H. Sun, M.F. Maitz, Phys. Rev. B 72 (2005) 1–9, 014120.
- [40] R. McCann, S.S. Roy, P. Papakonstantinou, I. Ahmad, P. Maguire, J.A. McLaughlin, L. Petaccia, S. Lizzit, A. Goldoni, Diamond Relat. Mater. 14 (2005) 1057–1061.
- [41] H.K. Jeong, H.J. Noh, J.Y. Kim, M.H. Jin, C.Y. Park, Y.H. Lee, EPL 82 (2008) 67004.